Article

Fuel cell electrode characterization using neutron scattering

Olaf Holderer [1], Marcelo Carmo[2] , Meital Shviro[2], Werner Lehnert[2,3], Yohei Noda[4] , Satoshi Koizumi[4] Marie-Sousai Appavou[1] , Marina Appel[1], and Henrich Frielinghaus[1]

1 Forschungszentrum Jülich, Jülich Centre for Neutron Science (JCNS) at MLZ, 85747 Garching, Germany; o.holderer@fz-juelich.de
2 Forschungszentrum Jülich, Institute of Energy and Climate Research (IEK-3), 52425 Jülich, Germany
3 RWTH Aachen University, Faculty of Mechanical Engineering, 52062 Aachen, Germany
4 Ibaraki University, D302 IQBRC 162-1, Shirakata, Tokai-mura, Naka-gun, Ibaraki, Japan
* Correspondence: o.holderer@fz-juelich.de

Version February 28, 2019 submitted to Preprints

Abstract: Electrochemical energy conversion and storage is key for the use of regenerative energies at large scale. A thorough understanding of the individual components, such as the ion conducting membrane and the electrode layers, can be obtained with scattering techniques on atomit to molecular length scales. The largely heterogeneous electrode layers of High-Temperature Polymer Electrolyte Fuel Cells are studied in this work with small- and wide-angle neutron scattering at the same time with the iMATERIA diffractometer at the spallation neutron source at J-PARC, opening a view on structural properties on atomic to mesoscopic length scales.

Keywords: SANS; WANS; HT-PEFC; electrode layer

1. Introduction

Electrochemical energy conversion plays an important role for the current change in energy infrastructure. Fuel cells provide a clean way of electricity production from chemical energy, e.g. for the automotive sector or also stationary sector from kW to MW energy scales [1]. The environmentally friendly production of hydrogen gas would allow to store "green energy" and to convert it back in times of high demand or low electricity production. Electrolyzers and fuel cells are the components capable of converting between electricity and H_2. The real world usage and operation of electrochemical energy converters depends strongly on the reliability of operation and the costs. A microscopic understanding of the transport processes is important in this context in order to optimize the different components of electrolyzers and fuel cells. At the heart of these devices is the ion conducting membrane, consisting of an polymer electrolyte membrane doped with phosphoric acid or potassium hydroxide, and the electrode layers around. X-ray and neutron radiography have been applied to high temperature polymer electrolyte membrane (PEM) fuel cells and electrolyzers to gain insight into the inner parts of the devices [2,3]. A powerful suite of experimental techniques for characterizing electrodes and membranes on microscopic time- and length-scales are neutron scattering experiments [4]. The wavelength of neutrons allows to look at structures from atomic to macroscopic length scales with different scattering [5,6] and imaging techniques [7,8]. Moreover, the kinetic energy of neutrons allows to study proton diffusion processes on nanometer length scales [9]. The large penetration through materials allows even for "operando" experiments with neutron spectroscopy [10]. Such advanced characterization methods shall permit researchers to increase cell efficiencies, unveil degradation mechanisms, and fabricate the next generation of solid electrolytes for fuel cells and electrolyzers. Here in this manuscript, another important step is given towards this direction, unveiling critical properties and characteristics using neutron scattering.

 doi:10.20944/preprints201903.0003.v1

2. Materials and Methods

2.1. Materials

In this contribution, electrode layers of HT-PEFCs are investigated. The gas diffusion elecrodes are prepared as described in Ref. [11–13] and for details we refer to this reference. In brief, Pt nanoparticles supported on carbon with 20 and 60 wt% Pt were dissolved and mixed with PTFE as an ink, which then was casted with a doctor blade technique onto a commercially available gas diffusion layer. Phosphoric acid doping of the electrode layer was aiming to an amount of approximately 10 μl PA per cm^2. A PA/ethanol solution (1:4 in volume) has been prepared and the corresponding amount of PA dropped onto the electrode layer.

2.2. Neutron Scattering

Neutron scattering experiments have been carried out at the iMATERIA beamline [14,15] at the Japanese spallation neutron source at J-PARC. The instrument covers a large range of scattering vectors, combining small angle and wide angle neutron scattering due to a large coverage with detectors and the inherent properties of a pulsed neutron source with a broad range of available neutron wavelengths with each pulse. The modulus q of the scattering vector ranges from q=10^{-2} - 4 Å^{-1}, covering length scales d=2π/q from atomic distances to about 100 nm.

2.3. Transmission Electron Microscopy

Dry membranes have been analyzed with a Transmission electron microscope (TEM). The images were obtained by using Thermo ScientificTM Titan 80-300 electron microscope equipped with a spherical aberration (Cs) corrector (CEOS) for the objective lens [16], and a JEM 2200 FS EFTEM instrument (JEOL, Tokyo, Japan) with zero-loss energy filtering. The sample preparation has been described in Ref. [13].

3. Results

We first address the structure of the Pt/C catalysts using Transmission Electron Microscopy (TEM). Figure 1 shows the bright field TEM images of a 20%wt. and a 60%wt. platinum supported on carbon black from Johnson&Matthey. The mean particle size was 2.6 and 3.5 nm for the 20% Pt/C and 60% Pt/C respectively. The nanoparticles are homogeneously dispersed over the entire carbon surface, and only scattered agglomerates are observed. However, it is clearly noticed on the 60% Pt/C (Figure 1B) that small nanoparticles tend to coalesce into larger particles or form agglomerates. Nevertheless, we consider both catalysts options suitable for electrode fabrication and further characterization.

While TEM gives an excellent impression on local length scales, scattering experiments provide the average information across the whole sample and are in this sense complementary. Secondly, also liquid components can be present in scattering experiments, therefore also phosphoric acid doped samples can be analyzed. Electrode layers with two different platinum catalyst loadings have been measured empty and loaded with phosphoric acid (PA). Figure 2 shows the results of the neutron scattering experiments with extended q-range for a catalyst loading of 20 %.

Preprints (www.preprints.org) | NOT PEER-REVIEWED | Posted: 1 March 2019 doi:10.20944/preprints201903.0003.v1

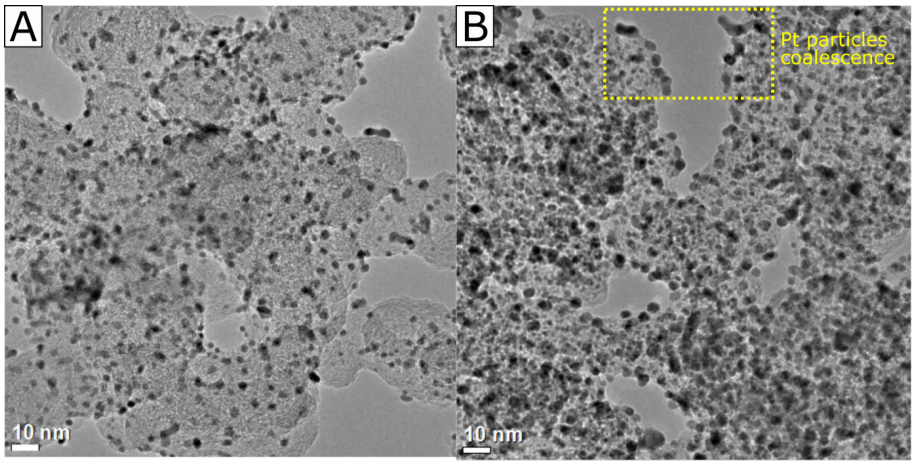

Figure 1. Bright-field TEM images of (a) 20%wt. Platinum supported on carbon black (Pt/C 20%), (b) 60%wt. Platinum supported on carbon black (Pt/C 60%), both catalysts commercially available from Johnson&Matthey. Pt/C 20% has an average particle size of 2.6 nm $\pm$ 0.5, and Pt/C 60% has an average particle size of 3.5 nm $\pm$ 0.5.

A generic way of SANS data evaluation is provided by the Beaucage model [17,18]:

$$I_B(q) = G\exp(-q^2R_g^2/3) + B\left(erf\left(qR_g/\sqrt{(6)}\right)^3\right)^P \tag{1}$$

with a characteristic radius of gyration R_g and "Guinier-prefactor" G, and a power law decay with the Porod exponent P and scaling factor B, which can be written as

$$B = \frac{GP}{R_gP}\left(\frac{6P^2}{(2+P)(2+2P)}\right)^{P/2}\Gamma(P/2) \tag{2}$$

with the Gamma function $\Gamma(x)$. It yields a characteristic length scale via the radius of gyration, the power law decay P indicating the fractality of the structure.

The small angle part (corresponding to large structures) of the electrode layer has been evaluated with two levels of the Beaucage model plus a constant background which is mainly a result from isotropic incoherent scattering in the sample:

$$I_{SANS}(q) = I_{B1}(q) + I_{B2}(q) + bgr \tag{3}$$

where bgr is a constant and $I_{B1/2}(q)$ are two instances of the Beaucage model, yielding two characteristic length scales $R_{1/2}$.

The diffraction part (WANS, wide angle neutron scattering) of the scattering curve with q>1Å^{-1} has been fitted with a sum of Gaussians:

$$I_{WANS}(q) = \sum_i A_i \exp\left(-(q-q_i)^2/(2\sigma_i^2)\right) \tag{4}$$

The high-q regime has been fitted with i=4 Gaussians, yielding the peak area, the position of the peak and the standard deviation for the different peaks. This rather phenomenological approach is sufficient in this case since the visible peaks are attributed to different materials in the sample.

The whole scattering curve can be described finally with the two contributions from SANS and WANS:

$$I(q) = I_{SANS}(q) + I_{WANS}(q) \tag{5}$$

Preprints (www.preprints.org) | NOT PEER-REVIEWED | Posted: 1 March 2019 doi:10.20944/preprints201903.0003.v1

The available diffraction peaks are not sufficient for a crystallographic analysis and would mainly show the Pt structure as most crystalline component. We think therefore this procedure being adequate to identify the component and variations by analyzing the peak area of the respective contributions.

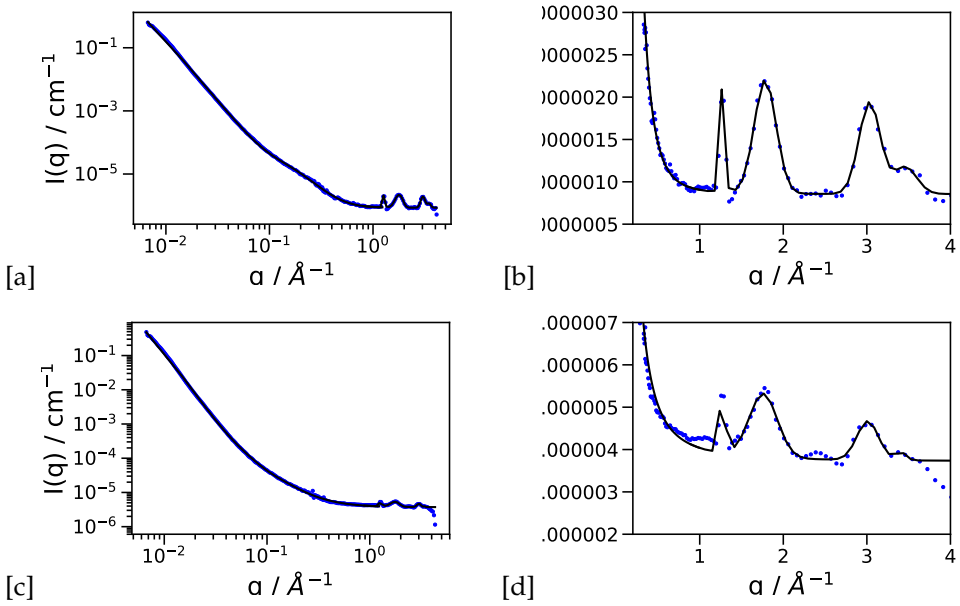

Figure 2. (**a**) SANS-WANS diffraction data for the empty 20 % platinum containing electrode layer (**b**) only the high-q region shown on a linear scale (**c**) the same sample filled with phosphoric acid (**d**) high-q region of the phosphoric acid doped electrode. The hydrogen contents is responsable for the higher incoherent background.

Table 1. SANS region with fit parameters for the evaluation with the Beaucage model with two characteristic length scales.

Parameter	Pure electrode 20 %	PA loaded electrode 20%	Pure electrode 60 %	PA loaded electrode 60 %
G_0(cm^{-1})	7.334e-06	4.060e-05	9.197e-06	1.684e-05
G_1 (cm^{-1})	2.442e+00	1.392e+00	1.902e+00	1.121e+00
bgr (cm^{-1})	2.331e-07	9.733e-07	2.664e-07	1.620e-06
$R_{g,0}$ (Å)	9.945e+00	2.908e+01	1.101e+01	1.663e+01
$R_{g,1}$ (Å)	4.915e+02	4.537e+02	5.670e+02	5.027e+02
P_0	3.634e+00	2.052e+00	4.029e+00	2.403e+00
P_1	3.847e+00	4.054e+00	3.793e+00	3.972e+00

Preprints (www.preprints.org) | NOT PEER-REVIEWED | Posted: 1 March 2019 doi:10.20944/preprints201903.0003.v1

Table 2. Diffraction region with q>1^{-1}. Peaks were fitted with Gaussian curves. The parameters are peak area A_i, peak postition q_i, standard deviaiton of the Gaussian σ_i

Parameter	Pure electrode 20 %	PA loaded electrode 20%	Pure electrode 60 %	PA loaded electrode 60 %
A_0 (cm^{-1})	1.259e-06	1.431e-06	7.926e-07	6.270e-07
q_0 ($Å^{-1}$)	1.271e+00	1.272e+00	1.270e+00	1.226e+00
σ_0 ($Å^{-1}$)	2.969e-02	3.758e-02	3.386e-02	1.439e-01
A_1 (cm^{-1})	1.344e-06	1.505e-06	1.161e-06	1.213e-06
q_1 ($Å^{-1}$)	1.784e+00	1.760e+00	1.807e+00	1.797e+00
σ_1 ($Å^{-1}$)	1.308e-01	1.675e-01	1.557e-01	2.075e-01
A_2 (cm^{-1})	1.086e-06	9.214e-07	7.273e-07	7.673e-07
q_2 ($Å^{-1}$)	3.034e+00	3.010e+00	3.198e+00	3.007e+00
σ_2 ($Å^{-1}$)	1.272e-01	1.285e-01	4.155e-01	2.372e-01
A_3 (cm^{-1})	3.201e-07	1.923e-07	5.341e-07	3.405e-07
q_3 ($Å^{-1}$)	3.459e+00	3.406e+00	3.985e+00	3.535e+00
σ_3 ($Å^{-1}$)	1.387e-01	-6.162e-02	5.440e-02	8.120e-02

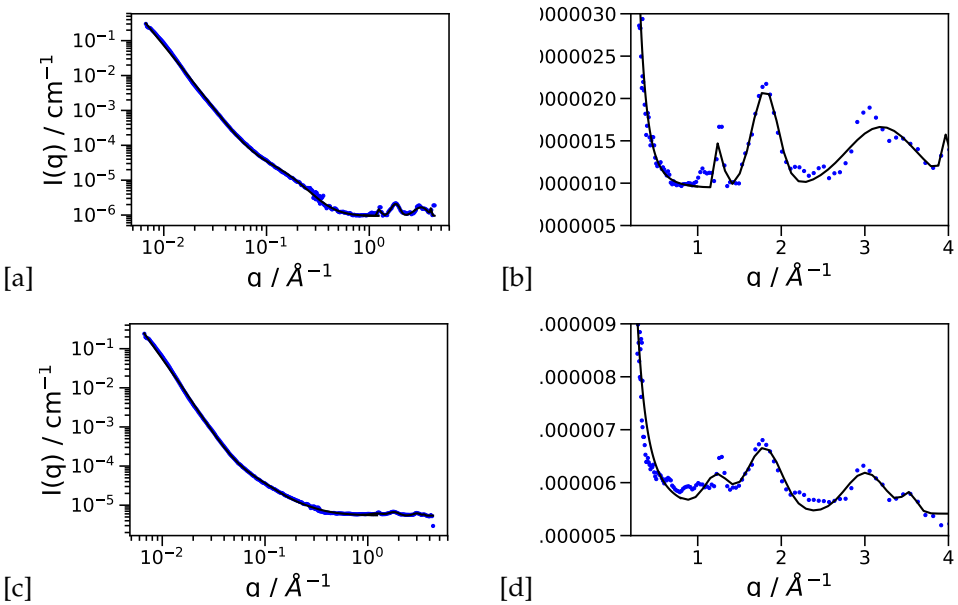

Figure 3. (**a**) SANS-WANS diffraction data for the empty 60 % platinum containing electrode layer (**b**) only the high-q region shown on a linear scale (**c**) the same sample filled with phosphoric acid (**d**) high-q region of the phosphoric acid doped electrode. The hydrogen contents is responsable for the higher incoherent background.

4. Discussion

The structure of HT-PEFC catalyst layers has been analyzed with SAXS, SANS and transmission electron microscopy (TEM) with samples of the same kind (20 and 60 % Pt) [13,19,20]. In these publications we have shown that the combination of different scattering methods highlights different parts of the sample. X-rays are mostly sensitive to heavy elements (as are electrons in TEM), thus highlighting the Pt catalyst, while neutrons have an irregular dependence of the scattering length on the element, with an additional isotope dependence, which allows for contrast variation by H-D exchange, e.g. with deuterated phosphoric acid. Especially in multicomponent systems this opens the way for highlighting different parts of the sample and getting in this way otherwise hidden details such as platinum particle size and agglomeration.

Here we want to point out the experimental advantage of covering the q-range from 1-1000 $Å^{-1}$ with the same sample. From the SANS regime, we observe the characteristic length scales with the

 doi:10.20944/preprints201903.0003.v1

2 instances of the Beaucage model, with $R_{g,0}$ of about 10 Å from the Pt particles, and a larger length scale $R_{g,1} \simeq 500$ Å of the supporting structure, with a fractal power law decay with an exponent P close to 4 indicating a compact structure. The phosphoric acid loaded samples show a slight increase in $R_{g,0}$. Since the incoherent background is much higher due to the larger hydrogen contents, we think that the slope P has to be taken with care in this case.

At q>1 $Å^{-1}$ we attribute the first peak (0) to the PTFE support present in the electrode ($q_0 \simeq 1.2$ $Å^{-1}$), the second peak (1) to the carbon support ($q_1 \simeq 1.8$ $Å^{-1}$), and peaks (2) and (3) to the Pt (111) and Pt (200) reflections. More Bragg peaks for a crystallographic analysis of the Pt particles are beyond the q-range of the experiment. We can see that the area of the peaks (A_i) is approximately constant between empty and PA loaded membranes (with the largest uncertainty on peak (3) at the edge of the experimental range. The area can be compared therefore under different conditions of electrolyte (PA) loading. The ratio of carbon to platinum peak would be a measure of possible degradation of catalyst particles if electrodes after some time of operation are compared to fresh electrodes. The size change the larger length scales of $R_{g,0}$ is an indication of arrangement of phosphoric acid adsorbed onto Pt particles, thus producing a larger spherical shell with a scattering length density (SLD) larger than the empty space around. This could be analyzed in a next step in a contrast variation series, where deuterated and protonated phosphoric acid are mixed in different ratios, such that the surrounding PA has different contrasts to e.g. the platinum catalysts ($SLD_{D_3PO_4}$=5.6x10^{-6} $Å^{-2}$, $SLD_{H_3PO_4}$=1x10^{-6} $Å^{-2}$, SLD_{Pt}=6.2x10^{-6} $Å^{-2}$). The combination of $R_{g,0}$ with the constant area of the Pt peak (3) suggests the adsorption of PA onto the Pt particles as a result of the broad range of length scales available in this experiment.

5. Conclusions

Neutron scattering provides a direct visualization window into the components of fuel cells and electrolyzers, here focused on electrode layers of high temperature PEM fuel cells. The heterogeneous structure over a wide range of length scales requires also experimentally that diffraction experiments are conducted over a broad range from atomic diffraction to mesoscopic SANS measurements (and possibly with radiography experiments to macroscopic length scales). This work showed that scattering experiments over a large range of length scales provide an insight into the individual components (catalyst particles, carbon structure) and investigate at the same time on larger scale the fractal structure of the electrode material and its evolution upon filling with electrolyte. Varying the contrast with H-D exchange allows to highlight different parts of the sample and distinguish structural properties of different materials, which will be further elaborated in the future. This is especially useful for such heterogeneous systems as electrode layers. As a future plan, experiments using dynamic nuclear polarization combined with SANS [21,22] are planned, where contrast variation is achieved in industrial type heterogeneous samples by polarizing the proton spin in the sample.

Author Contributions: conceptualization, O.H.. and H.F., W.L.; methodology, O.H., H.F., M.C. and W.L.; formal analysis, O.H. and Y.N.; investigation, O.H. and Y.N. and H.F. and M.-S. A. and M. A. and W. L. and M.S.; writing–original draft preparation, O.H..; writing–review and editing, O.H. and H.F. and W.L. and M.C.;

Funding: Please add: "This research received no external funding" or "This research was funded by NAME OF FUNDER grant number XXX." and and "The APC was funded by XXX". Check carefully that the details given are accurate and use the standard spelling of funding agency names at https://search.crossref.org/funding, any errors may affect your future funding.

Acknowledgments: In this section you can acknowledge any support given which is not covered by the author contribution or funding sections. This may include administrative and technical support, or donations in kind (e.g., materials used for experiments).

Conflicts of Interest: The authors declare no conflict of interest.

Abbreviations

The following abbreviations are used in this manuscript:

HT-PEFC	High Temperature Polymer Electrolyte Fuel Cell
PA	Phosphoric Acid
SLD	Scattering Length Density
TEM	Transmission Electron Microscopy
SANS	Small Angle Neutron Scattering
WANS	Wide Angle Neutron Scattering

1. Carrette, L.; Friedrich, K.; Stimming, U. Fuel cells–fundamentals and applications. *Fuel cells* **2001**, *1*, 5–39.
2. Arlt, T.; Lüke, W.; Kardjilov, N.; Banhart, J.; Lehnert, W.; Manke, I. Monitoring the hydrogen distribution in poly (2, 5-benzimidazole)-based (ABPBI) membranes in operating high-temperature polymer electrolyte fuel cells by using HD contrast neutron imaging. *Journal of Power Sources* **2015**, *299*, 125–129.
3. Maier, W.; Arlt, T.; Wannek, C.; Manke, I.; Riesemeier, H.; Krüger, P.; Scholta, J.; Lehnert, W.; Banhart, J.; Stolten, D. In-situ synchrotron X-ray radiography on high temperature polymer electrolyte fuel cells. *Electrochemistry Communications* **2010**, *12*, 1436–1438.
4. Kearley, G.J.; Peterson, V.K. *Neutron applications in materials for energy*; Springer, 2015.
5. Babcock, E.; Szekely, N.; Konovalova, A.; Lin, Y.; Appavou, M.S.; Mangiapia, G.; Revay, Z.; Stieghorst, C.; Holderer, O.; Henkensmeier, D.; Lehnert, W.; Carmo, M. Using neutron methods SANS and PGAA to study evolution of structure and composition of Alkali-doped Polybenzimidazole membranes. *Journal of Membrane Science* **2019**.
6. Ivanova, O.; Lüke, W.; Majerus, A.; Krutyeva, M.; Szekely, N.; Pyckhout-Hintzen, W.; Appavou, M.S.; Monkenbusch, M.; Zorn, R.; Lehnert, W.; others. Influence of morphology on physical properties of poly (2, 5-benzimidazole) membranes. *Journal of Membrane Science* **2017**, *533*, 342–350.
7. Manke, I.; Hartnig, C.; Grünerbel, M.; Kaczerowski, J.; Lehnert, W.; Kardjilov, N.; Hilger, A.; Banhart, J.; Treimer, W.; Strobl, M. Quasi–in situ neutron tomography on polymer electrolyte membrane fuel cell stacks. *Applied Physics Letters* **2007**, *90*, 184101.
8. Hoeh, M.A.; Arlt, T.; Kardjilov, N.; Manke, I.; Banhart, J.; Fritz, D.L.; Ehlert, J.; Lüke, W.; Lehnert, W. In-operando neutron radiography studies of polymer electrolyte membrane water electrolyzers. *ECS transactions* **2015**, *69*, 1135–1140.
9. Hopfenmüller, B.; Zorn, R.; Holderer, O.; Ivanova, O.; Lehnert, W.; Lüke, W.; Ehlers, G.; Jalarvo, N.; Schneider, G.J.; Monkenbusch, M.; others. Fractal diffusion in high temperature polymer electrolyte fuel cell membranes. *The Journal of chemical physics* **2018**, *148*, 204906.
10. Khaneft, M.; Shuai, L.; Lin, Y.; Janßen, H.; Lüke, W.; Zorn, R.; Ivanova, O.; Radulescu, A.; Holderer, O.; Lehnert, W. Proton dynamics of phosphoric acid in HT-PEFCs: Towards "operando" experiments. AIP Conference Proceedings. AIP Publishing, 2018, Vol. 1969, p. 030003.
11. Wannek, C.; Lehnert, W.; Mergel, J. Membrane electrode assemblies for high-temperature polymer electrolyte fuel cells based on poly (2, 5-benzimidazole) membranes with phosphoric acid impregnation via the catalyst layers. *Journal of Power Sources* **2009**, *192*, 258–266.
12. Carmo, M.; Keeley, G.P.; Holtz, D.; Grube, T.; Robinius, M.; Müller, M.; Stolten, D. PEM water electrolysis: Innovative approaches towards catalyst separation, recovery and recycling. *International Journal of Hydrogen Energy* **2019**.
13. Khaneft, M.; Holderer, O.; Ivanova, O.; Lüke, W.; Kentzinger, E.; Appavou, M.; Zorn, R.; Lehnert, W. Structure and Proton Dynamics in Catalytic Layer of HT-PEFC. *Fuel Cells* **2016**, *16*, 406–413.
14. Ishigaki, T.; Hoshikawa, A.; Yonemura, M.; Morishima, T.; Kamiyama, T.; Oishi, R.; Aizawa, K.; Sakuma, T.; Tomota, Y.; Arai, M.; others. IBARAKI materials design diffractometer (iMATERIA)—Versatile neutron diffractometer at J-PARC. *Nuclear Instruments and Methods in Physics Research Section A: Accelerators, Spectrometers, Detectors and Associated Equipment* **2009**, *600*, 189–191.
15. Koizumi, S.; Yohei, N. A Variety of Small-angle Neutron Scattering Instruments Available in Tokyo Area, Japan. - Complimentary Use of Accelerator and Reactor. JPS Conference Proceedings, 2019, p. in press.
16. Thust, A.; Barthel, J.; Tillmann, K. FEI Titan 80-300 TEM. *Journal of large-scale research facilities JLSRF* **2016**, *2*, 41.
17. Hammouda, B. Analysis of the Beaucage model. *Journal of Applied Crystallography* **2010**, *43*, 1474–1478.

 doi:10.20944/preprints201903.0003.v1

18. Beaucage, G. Approximations leading to a unified exponential/power-law approach to small-angle scattering. *Journal of Applied Crystallography* **1995**, *28*, 717–728.
19. Holderer, O.; Khaneft, M.; Lin, Y.; Liu, S.; Feoktystov, A.; Kruteva, M.; Zorn, R.; Lehnert, W. Nanostructure of HT-PEFC Electrodes Investigated with Scattering Methods. *ECS Transactions* **2017**, *80*, 19–25.
20. Holderer, O.; Ivanova, O.; Khaneft, M.; Hopfenmüller, B.; Lüke, W.; Majerus, A.; Appavou, M.S.; Szekely, N.; Krutyeva, M.; Kentzinger, E.; others. Local Structure and Proton Transport in HT-PEFCs Measured with Neutron Scattering. *ECS transactions* **2015**, *69*, 337–343.
21. Noda, Y.; Kumada, T.; Hashimoto, T.; Koizumi, S. Inhomogeneous dynamic nuclear polarization of protons in a lamella-forming diblock copolymer investigated by a small-angle neutron scattering method. *Journal of Applied Crystallography* **2011**, *44*, 503–513.
22. Noda, Y.; Koizumi, S.; Masui, T.; Mashita, R.; Kishimoto, H.; Yamaguchi, D.; Kumada, T.; Takata, S.i.; Ohishi, K.; Suzuki, J.i. Contrast variation by dynamic nuclear polarization and time-of-flight small-angle neutron scattering. I. Application to industrial multi-component nanocomposites. *Journal of applied crystallography* **2016**, *49*, 2036–2045.